JOURNAL OF PROPULSION AND POWER
Vol. 13, No. 2, March–April 1997

Mixing Characteristics of Forced Mixers with Scalloped Lobes

Simon C. M. Yu,* T. H. Yip,† and C. Y. Liu‡
Nanyang Technological University, Singapore 639798, Singapore

An experimental investigation has been undertaken to study the mixing characteristics of forced mixers with scalloped lobes using a two-component fiber-optic laser Doppler anemometer at a Reynolds number of 2.27×10^4 and at a velocity ratio 1:2 across the lobes. The trailing edge of the mixers, without scalloping, had the shape of a square wave, a semicircular wave, and a triangular wave. Scalloping was achieved by eliminating up to 70% of the sidewall area at the penetration region of each lobe. The aspect ratio of each lobe (lobe height-to-wavelength ratio) was at unity and the half-angles at the penetration region were 22 and 35 deg for the scalloped and the aggressively scalloped mixers, respectively. The wavelength and lobe height were the same for both types of mixer. The results showed that lobe configurations appeared to be more important than the penetration angles for the benefit of scalloping to occur. Strengths of the streamwise circulation near the trailing edge for respective scalloped mixers were higher than the nonscalloping cases, largely because of the formation of two pairs of streamwise vortices at each lobe. The subsequent decay rates with downstream distance were also found to be more rapid, indicating that a faster mixing rate can actually be achieved by the scalloped mixers. Additional production of turbulent kinetic energy appeared at about two to three wavelengths downstream of the trailing edge and then asymptote to lower level in the far-field region. Spatial uniformity of the mass flux at the wake region could be achieved at two wavelengths further downstream of the high turbulent kinetic energy region.

Nomenclature

A_{wake} = cross-sectional area bounded by the wake region
C_1 = normalized streamwise circulation, $\Gamma_s/U_r h \tan \varepsilon$
H = boundary-layer shape factor, δ^*/Θ
h = lobe height, 33 mm
k = turbulent kinetic energy, $\frac{1}{2}(u'^2 + v'^2 + w'^2)$
Re = Reynolds number, $U_r\lambda/\upsilon = 2.27 \times 10^4$
Re_Θ = Reynolds number based on the momentum thickness
SF = shape factor for the mass flux, $\int U \, dA_{wake}/UrA_{wake}$
U, u' = streamwise mean and the corresponding rms velocities
U_{max} = maximum velocity of the local stream
U_r = reference mean velocity, $(U_1 + U_2)/2 = 10$ m/s
U_s = secondary mean velocity, $\sqrt{V^2 + W^2}$
U_1, U_2 = mean velocity of the top and bottom streams
$\overline{uv}, \overline{uw}$ = Reynolds shear stresses
V, v' = horizontal mean and the corresponding rms velocities
W, w' = vertical mean and the corresponding rms velocities
x, y, z = streamwise, horizontal, and vertical directions
Γ_s = streamwise circulation
δ^* = displacement thickness, mm
ε = half of the included divergent angle of the penetration region, 22 and 35 deg for the scalloped lobed mixer and the aggressively scalloped lobed mixer, respectively
Θ = momentum thickness, mm
θ = shear-layer entrainment momentum thickness, mm
λ = nominal lobe wavelength, 33 mm
υ = kinematic viscosity

Presented as Paper 96-0117 at the AIAA 34th Aerospace Sciences Meeting and Exhibit, Reno, NV, Jan. 15–19, 1996; received Feb. 1, 1996; revision received Sept. 8, 1996; accepted for publication Sept. 19, 1996. Copyright © 1996 by the American Institute of Aeronautics and Astronautics, Inc. All rights reserved.

*Senior Lecturer, Thermal and Fluids Engineering Division, School of Mechanical and Production Engineering. Member AIAA.

†Research Student, Thermal and Fluids Engineering Division, School of Mechanical and Production Engineering.

‡Professor and Head of Division, Thermal and Fluids Engineering Division, School of Mechanical and Production Engineering. Member AIAA.

I. Introduction

THE mixing characteristics of lobed forced mixers and their advantages over the conventional nozzle designs in the application of turbofan engine exhausts have been investigated extensively.[1–3] These investigations showed that the enhanced mixing between the core and the bypass flows caused by the lobed mixer, not only reduced the jet noise, but also provided some gains on the net thrust.

The details of the lobed mixer flowfield by which the mixing enhancement may be attributed to, have also been investigated.[4–9] All of these investigations concluded that the mixing enhancement was essentially a result of the large mixing scales generated by the streamwise vortices shed downstream and the increase in the interfacial area, as a consequence of the convoluted trailing edge. Their measurements also showed that high strength of the streamwise vorticity shed by a lobe, together with a large velocity ratio across the lobe, would further enhance the mixing rate. However, the strength of the streamwise vorticity shed by a particular lobe configuration at the trailing edge did not increase significantly at higher velocity ratios.[15] Furthermore, the strength of the streamwise vorticity also showed a strong dependence on the geometry, such as the lobe shapes and the penetration angles.[8]

The inviscid nature of the streamwise vortices formation at the mixer trailing edge was first established by Barber et al.[5] They compared the streamwise circulation measurements near the trailing edge with the analytical results obtained based on the principle of two-dimensional continuity within the penetration region, and good agreement was obtained. Barber et al.[5] further showed that lobes consisting of straight parallel sidewalls were far superior to other geometries, in terms of maximizing strength of the streamwise vorticity at the trailing edge. There is little benefit, however, of increasing the penetration angle above 30 deg because of the possible boundary-

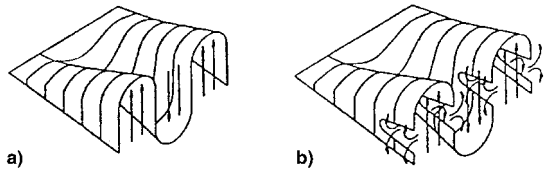

Fig. 1 Lobe scalloping effects (taken from Ref. 3): a) conventional and b) scalloped lobes.

layer separation at the penetration region, which would result in a substantial loss in the streamwise vorticity strength.[10] The penetration angle may increase to above 35 deg using the scalloped lobes. Presz et al.[3] has shown that using the scalloped lobes in a lobed mixer of aggressive penetration angles (>30 deg) can actually reduce the likelihood of boundary-layer separation. In the ejector application, the scalloped mixer can help to produce pumping performance, approaching ideal values.

The investigation of Presz et al.[3] suggested that additional streamwise vortices would be formed as a result of the scalloping, and thereby, promoted mixing (see Fig. 1). However, no detailed investigation has yet been carried out to study the flow characteristics of the scalloped mixers. Thus, the present investigation not only aims to elucidate the flow characteristics of the scalloped lobed mixers, but also to provide some information on the benefit of using the scalloped lobes.

The trailing edge shape of the scalloped mixers under investigation consists of square, semicircular, and triangular waves. The mixing characteristics of the corresponding nonscalloped mixers were reported previously by Yu et al.,[8] so that some comparisons can be made with the present investigations. Scalloped mixers at a larger penetration angle (35 deg), but at the same wavelength and lobe height, have also been studied.

The following section describes briefly the experimental setups for the velocity measurement purposes, including the laser Doppler anemometer (LDA). It will be followed by presentation and discussion of the results. This paper ends with a summary of important findings. Because of limited space, results for the flow visualization tests will not be reported here, but can be found in the conference version of this article.

II. Flow Configurations and Instrumentation

A. Lobed Mixer Configurations

Two types of lobed mixers were used in the present investigation, namely, the scalloped and the aggressively scalloped lobed mixers. They will be referred to as the *S* and the *AS* types of lobed mixers, respectively, in the subsequent sections. The nonscalloped mixers of Ref. 8 will be referred to as the *NS* type. Each mixer was made of 1.5-mm-thick fiberglass with six full lobes. The nominal wavelength for the *S* and *AS* types of lobed mixers is the same: 33 mm. The aspect ratio of each lobe (lobe height-to-wavelength ratio) was at unity, and the half-angles at the penetration region were 22 and 35 deg for the *S* and *AS* mixers, respectively (Figs. 2a and 2b).

The trailing edges of the mixers, without scalloping, had the shape of square, semicircular, and triangular waves. Scalloping was achieved by eliminating up to 70% of the sidewall area at the penetration region of each lobe. The coordinate system adopted in the present experiment is shown in Fig. 2a.

B. Wind Tunnel

The wind tunnel used for velocity measurements in the present investigation was similar to that used by Yu et al.,[8] but with a splitter plate dividing the contraction section equally into two halves (Fig. 2c). The model lobed mixer was mounted at the end of the splitter plate on entry to the test section. The arrangement was to ensure relatively low freestream turbulence levels (<0.5% of the local mean velocity) on entry to the test section on either side of the mixer. The Plexiglas® test section was 200 mm high, 200 mm wide, and 500 mm long.

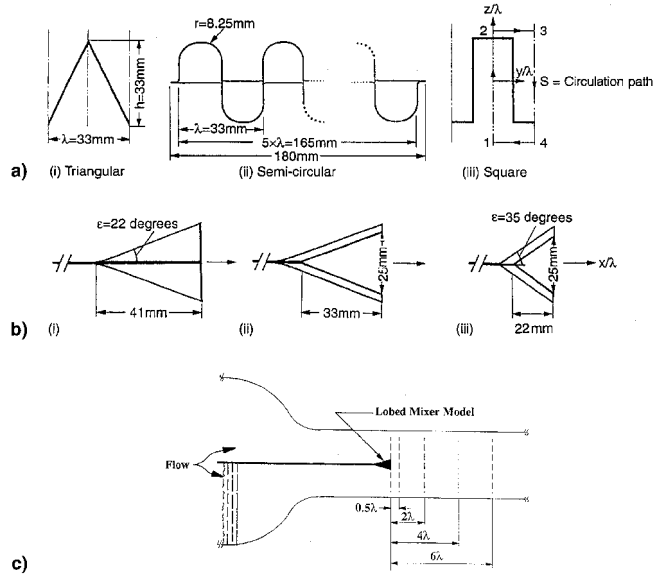

Fig. 2 a) End views for the lobed mixer trailing edges: (i) triangular, (ii) semicircular, and (iii) square; b) side views for the (i) nonscalloped, (ii) scalloped, and (iii) aggressively scalloped mixers; and c) schematic of the wind-tunnel facilities.

Different velocity ratios between the upper and lower streams were achieved by incorporating clothes and wire meshes on the lower half of the contraction section. In the present investigation, a mean speed of 10 m/s was used, corresponding to a Re of 2.27×10^4 for both the *S* and *AS* mixers, respectively (based on the nominal wavelength of the lobe at 33 mm). According to the previous work of Manning,[11] the mixing characteristics of a lobed mixer should become independent of the Reynolds number when it is above 1.2×10^4.

C. LDA

A three-beam, two-component, fiber-optic LDA (Dantec 55X series), with a 3-W argon laser operating in a backward-scattered mode, had been used to measure respective velocity components. A focusing lens of 400 mm provided a measuring probe volume of $0.11 \times 0.11 \times 2.4$ mm in the vertical direction and $0.12 \times 0.12 \times 2.5$ mm in the horizontal direction. The fiber-optic probe was mounted on an automated two-dimensional traversing system with an accuracy of ± 0.001 mm. Bragg shifting of frequency up to 2 MHz (on each channel) was used to avoid directional ambiguity. The Doppler signals were detected by photomultipliers and processed by counter-type signal processors. Fine solid particles, sizes within 5–10 μm generated by a commercially particles dispenser (PALAS RGB-1000), were used to seed the flow. At each measuring point, the mean velocities, the rms of the velocity fluctuations, and the Reynolds shear stresses were determined from populations of more than 2000 (on each channel) samples together with a coincidence window of 30 μs. Other coincidence window widths from 30 to 100 μs were also tested, but no significant differences in the results were found. Each individual measurement was required to satisfy the counter 5/8 validation comparison within a preset tolerance of 3%.

A careful appraisal on the errors associated with the LDA system was performed. The sources of error mainly stemmed from velocity biasing,[12] velocity gradient broadening,[13] the accuracy of the signal processor, and the finite sampling size.[14] Thus, the accuracy of the measured velocity components (normalized by the bulk mean velocity of the two streams, U_r, 10 m/s) can be expected to be about 2%, that of the rms of the velocity fluctuations (normalized by U_r) about 3%, and the Reynolds shear stresses (normalized by U_r^2) is expected to be about 5%, based on a 95% confidence level.

Measurements of the three-orthogonal mean velocities, U, V, and W; their corresponding rms fluctuations, u', v', and w'; and Reynolds shear stresses, $\overline{uv}$, $\overline{uw}$, were acquired in the projected area corresponding to the one lobe located close to the center of the test section, i.e., at the third lobe from the sidewall of the test section, and at downstream locations where x/λ = 0.5, 1, 2, 3, 4, 5 [the 1, 3, and 5 measurements were only obtained along the streamwise circulation path, as shown in Fig. 2a(iii)], and x/λ = 6 (see Fig. 2c). At each station, there were about 81 measuring points.

III. Results and Discussion

A. Initial Conditions

The velocity profiles on either side of the lobed mixer, measured at three wavelengths upstream of the penetration region for the three cases, were less than 1/10λ (boundary layer defined at $0.99U_{max}$). The calculated boundary-layer parameters are shown in Table 1, where Re_Θ represents the Reynolds number based on the momentum thickness. Both boundary-layer parameters and boundary-layer profiles indicated that the boundary layers on either side of the lobed mixer were turbulent ($\delta^*/\Theta \sim 1.3$). Streamwise turbulence levels outside the boundary-layer region had maximum values of 0.5% (normalized by the mean velocity of the local stream) and rose to about 15% close to the splitter plate on either side of the lobed mixer.

Downstream development of the streamwise and secondary flow velocities for respective lobed mixers are presented as isocontours and vectors, respectively. Further presentation of the results are in terms of the global quantities (such as the turbulent kinetic energy) obtained by averaging over a transverse plane and at successive downstream locations within the wake region. The wake region boundary may be defined at the region bounded by $0 < z/\lambda < 0.5$ and at the locations along the y/λ direction, where U_2/U_{r2} and $U_1/U_{r1} < 0.95$.

B. Downstream Development for the Mean Velocities

Only the results for the aggressively scalloped mixers are presented here. Contours of the normalized streamwise mean velocity U/U_r, and the corresponding secondary flow velocity vectors ($U_s/U_r = \sqrt{V^2 + W^2}/U_r$, arrow base is at the measuring point and at successive downstream stations), are shown in Figs. 3–5.

For the square mixer, the distribution of the streamwise mean velocity contours at x/λ = 0.5 (Fig. 3a) clearly shows that the influence of the secondary vortices the wake shed by the straight ends have shifted more toward the low speed side of the lobe. Two pairs of contrarotating vortices have been formed at each lobe with centers of the core located at around $y/\lambda = \pm 0.25$ and $z/\lambda = \pm 0.25$, as indicated clearly by the transverse streamlines plot in Fig. 3a. Absolute magnitude of the secondary flow velocities is some 30% higher than that in the *NS* case, but it is similar to that measured in the *S* case. At x/λ = 2 and Fig. 3b, the secondary motion continues to convect the fluids from the high-speed side to the center region, i.e., at around y/λ = 0.0 and z/λ = 0.0, but the magnitude of the secondary flow velocities at this location reduces substantially by almost 40% compared to that measured at the preceding station. The trace of the secondary vortices, however, remains obvious, and steep streamwise velocity gradients also appear along the $+z/\lambda$ and $\pm y/\lambda$ directions. By x/λ = 4 and Fig. 3c, a fairly uniform distribution of the velocity contours along the y/λ direction can be found, and the trace of the secondary vortices is no longer visible. By station x/λ = 6 and Fig. 3d, the strength of the secondary flow velocities at this location reduces further to less than 10% of that measured at x/λ = 0.5.

Table 1 Boundary-layer parameters at three wavelengths upstream of the penetration region

Velocity ratio 1:2	δ, mm	Θ, mm	H	Re_Θ
Top stream	0.52	0.39	1.33	193
Bottom stream	0.38	0.29	1.31	66

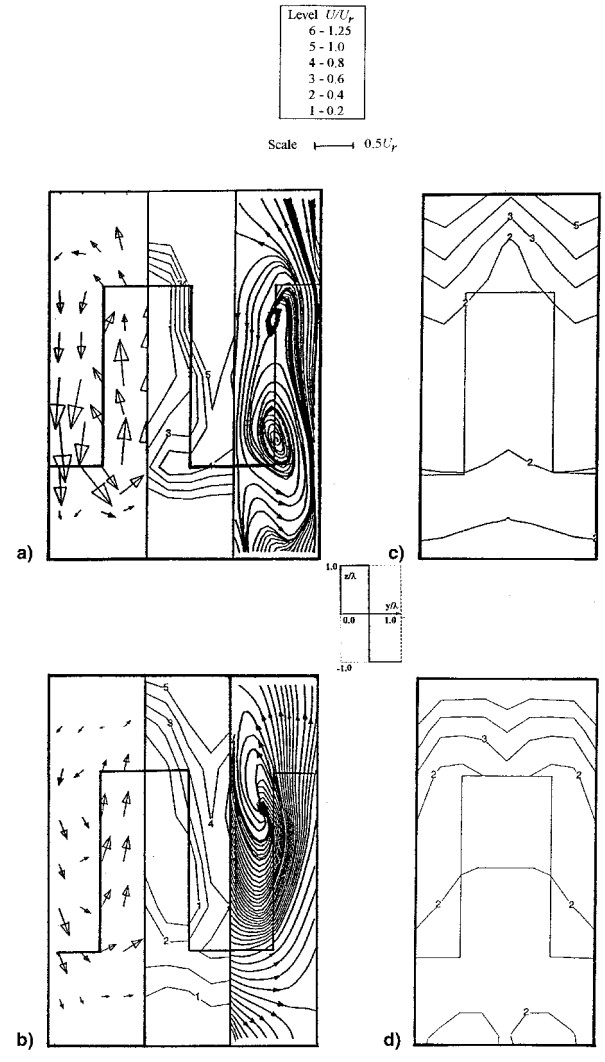

Fig. 3 Contours of the normalized streamwise velocity and the corresponding secondary velocity vectors at successive downstream stations for the *AS* square mixer. x/λ = a) 0.5 (with transverse streamlines plot), b) 2 (with transverse streamlines plot), c) 4, and d) 6.

Similar trends for the flows in the semicircular mixers can be found in Figs. 4a–4d. Four cross-stream vortices are also observed at each lobe with centers around the lobe peak and trough regions (see Fig. 4a). Absolute strength of the secondary flow velocities, in general, is not as high as that measured at the corresponding location in the square mixer. The contrarotating vortices cause distortion to the streamwise velocity contours at x/λ = 2.0 and Fig. 4b, particularly near the lobe trough regions. The vortex that appeared near the lobe peak region at x/λ = 0.5 is found almost dissipated at this station. One plausible reason for this observation may be that since this vortex is situated close to the high-speed region of the flow, during the mixing process, the even-out action of the velocity distribution within the lobe would lead to a decrease in the magnitude of the streamwise velocity at the corresponding region. This results in a vortex compression in the streamwise direction: the corresponding strength of the secondary vortex would thus be reduced. Uniformity of the velocity contours along the y/λ direction appears at x/λ = 4 and Fig. 4c. The vortices near the lobe peak region have almost dissipated, whereas those that appeared near the lobe troughs are still visible. Uniformity of the velocity contours along the y/λ di-

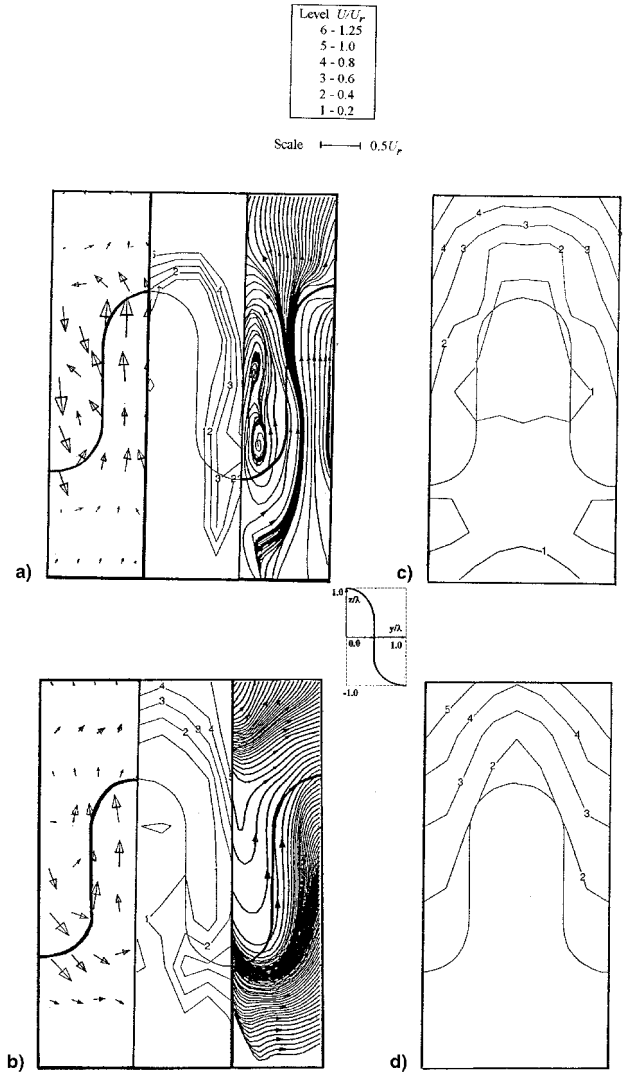

Fig. 4 Contours of the normalized streamwise velocity and the corresponding secondary velocity vectors at successive downstream stations for the *AS* semicircular mixer. x/λ = a) 0.5 (with transverse streamlines plot), b) 2 (with transverse streamlines plot), c) 4, and d) 6.

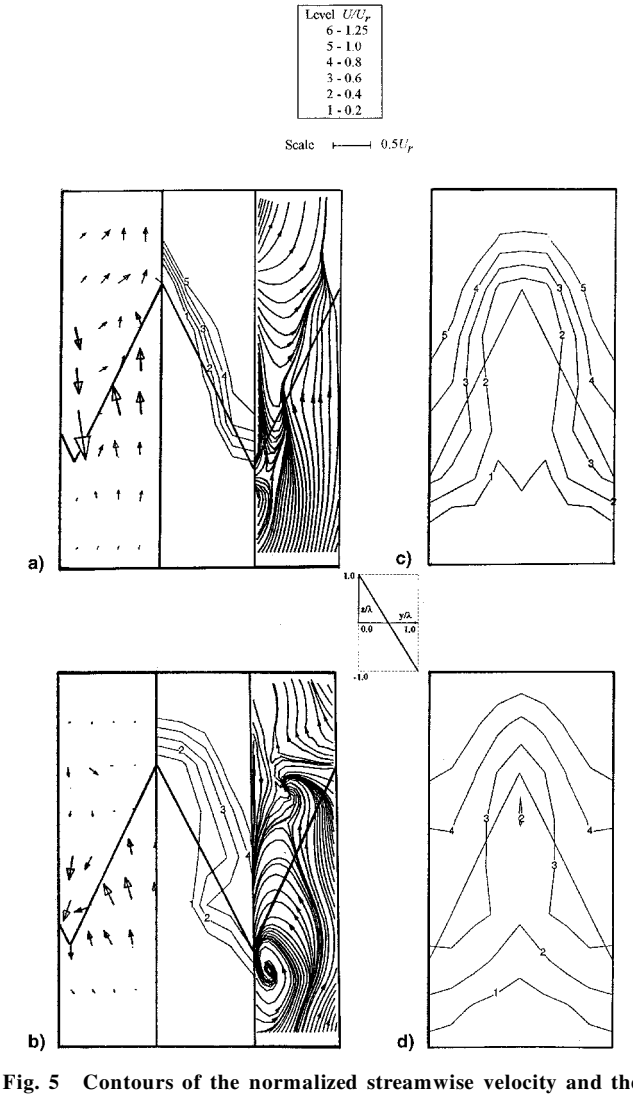

Fig. 5 Contours of the normalized streamwise velocity and the corresponding secondary velocity vectors at successive downstream stations for the *AS* triangular mixer. x/λ = a) 0.5 (with transverse streamlines plot), b) 2 (with transverse streamlines plot), c) 4, and d) 6.

rection appear at $x/\lambda = 6$, accompanied by the disappearance of all the secondary vortices (see Fig. 4d).

The formation of the vortices near the peak and trough regions can be more clearly seen in the results of the triangular mixers where the strength of the secondary flow velocities generated by the lobe itself is relatively weaker than the other two configurations. Figures 5a and 5b show the formation of the streamwise vortices: one appears near the lobe peak while the other one appears near the lobe trough. The sense of rotation for each vortex within a half-lobe is the same as the vortex generated by the lobe itself. Some distortions on the wake contours appear at the corresponding regions, but they are not as significant as those found in the other two configurations. The strength of the secondary flow velocities is also much lower than the other two configurations, by almost 50%, but is similar to that measured in the corresponding *NS* case. The results thus suggest that the increase in penetration angle and the scalloping have no significant impact on the triangular mixers. Some uniformity of the velocity contours along the y/λ direction is achieved by $x/\lambda = 6$, and the secondary vortices are almost dissipated (see Fig. 5d).

Based on the flow visualization results and the velocity measurements, a schematic view of the vortical structure in the vicinity of the scalloped mixer trailing edge may be constructed and is shown schematically in Figs. 6a and 6b. Within the range of $x/\lambda = 0.5$ from the trailing edge, two pairs of contrarotating vortices would be expected at each lobe's peak and trough regions [see Figs. 6a and 6b(i)]. The situation is reminiscent of the flows behind a delta wing at angles of incidence, in addition to the one that generated by the lobe itself. However, within a half-lobe, instead of finding three vortices, only two vortices are observed in the velocity measurements at $x/\lambda = 0.5$. It is therefore likely that the vortex generated by the lobe merges initially with one of the smaller vortices [the lower one in Fig. 6b(i)] to form a larger vortex, since they both have the same sense of rotation [see Fig. 6b(ii) (cf., Figs. 3a and 4a)]. Although the two vortices within a half-lobe are relatively smaller than the one that appeared in the nonscalloping case, it should be noted that the mixing scales of the two vortices are also smaller (but stronger in strength), thus making the scalloped mixer a more effective mixing device. After $x/\lambda = 1$, the remaining two vortices within a half-lobe appear to merge into another vortex, as shown in Figs. 6b(iii) (cf., Figs. 3b and 4b). Thus, the scalloping effects may only be clearly observed within the range of one wavelength downstream of the trailing edge.

C. Downstream Variation of the Streamwise Vorticity

The strength of the streamwise vorticity, which may be considered as one of the most important parameters to quantify

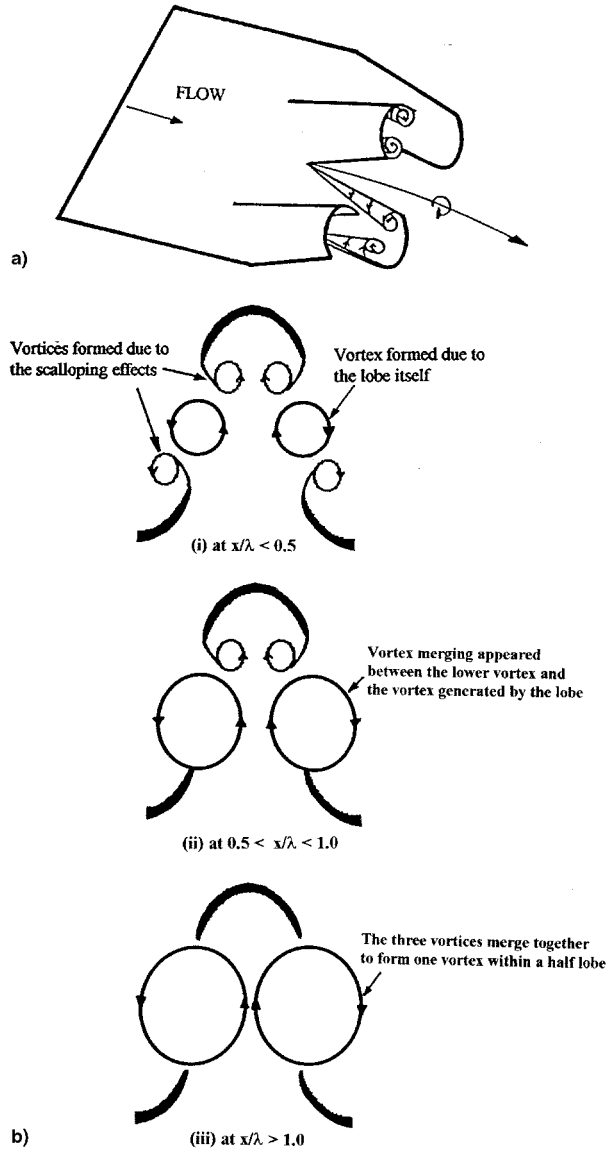

Fig. 6 Schematic of the vortical structure in the vicinity of the mixer trailing edge: a) schematic view and b) endview, flow is emerging out of paper.

the effectiveness of mixer performance, may be evaluated using the following expression:

$$C_1 = \Gamma_s/Urh \tan \varepsilon \qquad (1)$$

where Γ_s can be determined from integration along a path encompassing one-half of a lobe

$$\underset{1-2}{\oint} \boldsymbol{W}\, ds + \underset{2-3}{\oint} \boldsymbol{V}\, ds + \underset{3-4}{\oint} \boldsymbol{W}\, ds + \underset{4-1}{\oint} \boldsymbol{V}\, ds$$

as shown in Fig. 2a(iii).

The results are shown in Figs. 7a–7c. Results obtained from the *NS* mixers at the same velocity ratio, but thicker initial boundary layers in Ref. 8, are also plotted in Fig. 7 for comparison. (Although the initial boundary layers in the present investigation were thinner than those in Ref. 8, based on the investigation of Ref. 15, thicker initial boundaries should lead to a faster decay rate for the streamwise vorticity. This may form some basis for the present comparison.)

Computed values near the trailing edge (at $x/\lambda = 0.5$) in Figs. 7a–7c for the *AS* lobes were found to be the largest for the

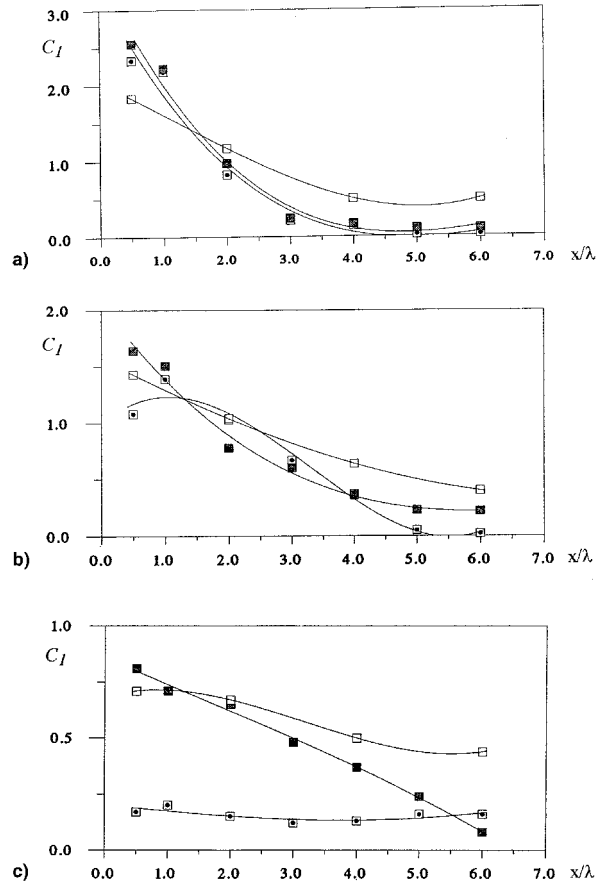

Fig. 7 Variation of the streamwise circulation with downstream distance: a) square, b) semicircular, and c) triangular mixers. ◉, scalloped; ■, aggressively scalloped; and □, nonscalloped.

square mixer followed by the semicircular and triangular mixers. A similar trend prevails in the results for the *S* and *NS* mixers.

For the square mixer and Fig. 7a, the decay rates for both the *S* and *AS* cases are very rapid in the first three wavelengths compared to the *NS* case. Downstream of three wavelengths, streamwise circulations for both *S* and *AS* cases have reduced to a negligible level, whereas the *NS* case is shown only to asymptote to lower values at the far-field region. It is expected that the rapid decaying nature for the *S* and *AS* cases should represent a more effective mixing process because of smaller, but stronger, mixing scales generated by the streamwise vortices. The magnitude of the streamwise circulation for the *AS* mixer at the trailing edge, as may be expected from the flow visualization results and velocity measurements, is only slightly higher than that of the *S* case. Although the *AS* mixer has a larger penetration angle, the effective length of the penetration region is shorter (about 50% shorter than the *S* cases); this may hamper the growth in strength for the secondary flow velocities.

For the semicircular mixers and Fig. 7b, the trailing-edge value for the *AS* case is found to be the largest, but the *S* case is lower than the *NS* case. There is an initial rise for the *S* case within the first one-and-a-half wavelengths, and it is followed by a relatively faster decay. The initial rise in the *S* case may be attributed to the fact that the four cross-stream vortices shed by the mixer did not achieve maximum strength until around $x/\lambda = 2.0$, whereas in the *AS* case, four fully grown vortices are formed immediately after the trailing edge. For the triangular mixers and Fig. 7c, the magnitude of the circulation for the *S* case is not as high as that of the *NS* case and can be attributed to the absence of the secondary vortices near the trailing edge. For the *AS* case, where the secondary vortices

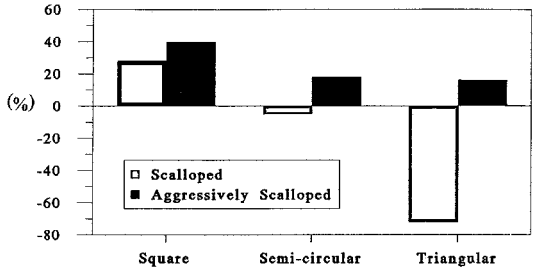

Fig. 8 Percentage of gain/loss in trailing-edge streamwise circulation strength for the *S* and *AS* mixers with respect to the *NS* mixers.

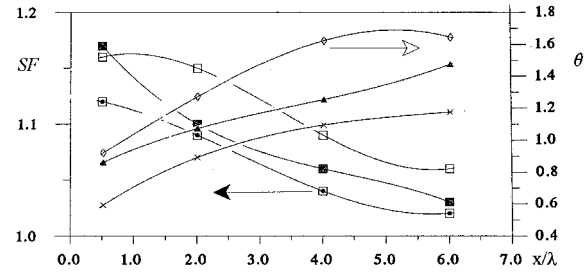

Fig. 9 Variation of the shape factor and momentum thickness with downstream distance. *SF*: ◉, square; ■, semicircular; and □, triangular. θ: ◇, square; , semicircular; and ×, triangular.

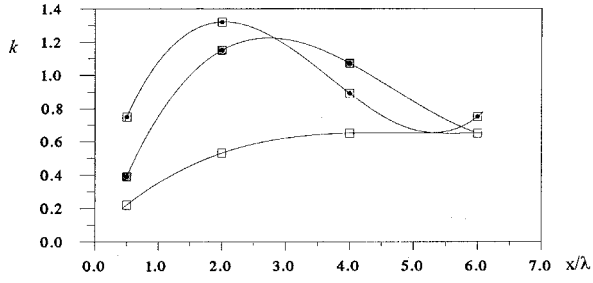

Fig. 10 Variation of the wake area averaged turbulent kinetic energy with downstream distance. ◉, square; ■, semicircular; and □, triangular.

are presented, it has a higher magnitude near the trailing edge and is followed by a relatively faster decay than the *NS* case.

Figure 8 summarizes the results for the overall gain (or loss) in streamwise circulation with respect to the *NS* cases at location $x/\lambda = 0.5$. The scalloping effects have increased the magnitude of the streamwise circulation for both the *S* and *AS* square mixers. While in the case of the semicircular mixer, only the *AS* case shows some increases. For the triangular mixers case, the substantial loss in the *S* case is largely because of the absence of streamwise vortices. There are some increases in the *AS* case, however, mixing by diffusion appears to be dominant.

D. Downstream Variation of the Spatial Uniformity and Shear-Layer Entrainment

In the present investigation, it may be sufficient to define completeness of mixing in terms of mass flux uniformity within the wake region, i.e.,

$$SF = \left(\int \frac{\rho U \, dA_{wake}}{\rho U r A_{wake}} \right) \tag{2}$$

Ideally, at the location where the top and bottom streams at the wake region of different velocities are to be completely mixed, the mass flux distribution would be very uniform and the shape factor should be at unity.

Figure 9 shows the variation of shape factor for the three *AS* mixers with downstream distance. The shape factors for the square and semicircular mixers show a decrease in the first three wavelengths downstream of the trailing edge, indicating a rapid variation of the momentum distribution within the wake region, as a consequence of streamwise vorticity shed by a lobe. In general, the square mixers can achieve uniformity faster than the other two configurations. Similar calculated values can also be found in the *S* cases. Thus, the results clearly suggested that for a particular scalloped lobed mixer configuration with a fixed lobe height and wavelength, the increase in penetration angle does not necessarily give rise to greater streamwise circulation strength.

The shear-layer growth rate with downstream distance, which quantifies the amount of fluid being entrained into the shear layer as a result of streamwise vorticity, may be evaluated in terms of momentum thickness,[7] i.e.,

$$\theta = \int \frac{(U - U_2)(U_1 - U)}{\Delta U r^2} \, dz \tag{3}$$

The results are also plotted in Fig. 9. The *AS* square mixer in the figure has the fastest growth rate in the first four wave lengths as a result of the highest streamwise vorticity shed by the lobe, followed by the semicircular and triangular mixers. Downstream of $x/\lambda = 4$, the growth rates for all cases decrease. This may be because the streamwise vortices at this location have been almost dissipated and the transverse momentum transport within the shear layer is dominated by the conventional gradient types of diffusion. At the location where the entrainment growth rate starts to decrease, the *SF* has also reached a steady level.

E. Downstream Variation of the Reynolds Stresses and Turbulent Kinetic Energy

Variation of the turbulent kinetic energy [$k = \frac{1}{2}(u'^2 + v'^2 + w'^2)$] is presented as an average over the wake region as a function of downstream distance, i.e.,

$$f\left(\frac{x}{\lambda}\right) = \int \frac{k \, dA_{wake}}{A_{wake}} \tag{4}$$

The variation of the transverse average of the turbulent kinetic energy for various mixers with distance downstream are found to be similar to the variation of the normal stresses. Peaks appeared within the range of $x/\lambda = 1.5$ to $x/\lambda = 2.0$ for both the (*S* and *AS* types) square and semicircular mixers, and a gradual decay followed. Only a gradual increase can be found in the triangular mixers within the range of measurement. The appearance of the peaks in Fig. 10 may be explained by examining the distribution of the Reynolds shear stresses ($\overline{uv}$ and $\overline{uw}$) and mean velocities at the corresponding location. High magnitude of the shear stresses appeared at regions of steep streamwise mean velocity gradients with a consequent higher production of turbulent kinetic energy. It appears that the additional production of the turbulent kinetic energy cannot be dissipated locally, and hence, gives rise to diffusion at the subsequent downstream stations. Thus, the initial generation of the streamwise vorticity by the lobe induced strong changes in the velocity field, which in turn, generated turbulence (at locations near the trailing edge) and enhanced the mixing at the downstream locations (at locations away from the trailing edge).

IV. Summary

The mixing characteristics of forced mixers with scalloped lobes has been investigated. The results were compared with the corresponding mixers without scalloping. The trailing edge configurations of the mixers, without scalloping, had the shape of square, semicircular, and triangular waves. Scalloping was achieved by eliminating up to 70% of the sidewall area at the

penetration region of each lobe. The results indicated that the lobe trailing-edge configurations may be more important than the penetration angles for the benefit of mixing enhancement caused by scalloping to occur.

Up to four cross-stream vortices were formed at each lobe near the trailing edge for the square and semicircular mixers. In the case of the triangular mixer, the streamwise vortices were absent in the *S* case. Although they appeared in the *AS* case, they were found to have minor effects on the mixing enhancement compared to the *NS* case. The dominant mixing mechanism appeared to be by diffusion, which was similar to that found in the *NS* case. Higher strength of the secondary flow velocities near the trailing edge, similar to those found in the *NS* cases, appeared in mixers with straight parallel sidewalls, i.e., in the (descending) order of the square, semicircular, and triangular mixers.

Strengths of the streamwise circulation near the trailing edge for both the *S* and *AS* types of lobed mixers (the square and semicircular) were found to be higher than the *NS* types, and the subsequent decay rates with downstream distance were also found to be more rapid. Spatial (mass flux) uniformity for the square and semicircular (both *S* and *AS* types) mixers can be achieved within three to four wavelengths downstream of the trailing edge. The locations of the peak in the variation of turbulent kinetic energy with downstream distance were found to appear at about two wavelengths upstream of the locations, where the strength of the streamwise circulation had almost dissipated and the spatial uniformity had almost reached a steady level. The initial generation of the streamwise vorticity by the lobe induced strong changes in the velocity field, which in turn, generated turbulence and enhanced the mixing. Thus, the mixing processes appeared to be dictated initially by the streamwise vorticity and were gradually taken over by the increased turbulent mixing.

No direct comparison can be made with the *NS* cases in the variation of the spatial uniformity with downstream distance because of the difference in the thicknesses of the upstream boundary layer. Based on the decay rate of the streamwise circulation with downstream distance, the results clearly suggested that using the scalloped lobes in both the square and semicircular mixers should be a more effective modification to promote mixing, given the same penetration angle, lobe height, and wavelength. Mixing in the present scalloped mixers should be more intense than the *NS* mixers, largely because the smaller (but stronger) sizes of the streamwise vortices represent mixing at a finer scale.

By keeping the same lobe height, but increasing the penetration angle to 35 deg, as in the *AS* cases, the magnitude of the trailing-edge streamwise circulation, however, did not increase significantly. The spatial uniformity could only be achieved at a location close to those achieved by *S* mixers. This may be largely because of a shorter effective length in the penetration region that may hamper the growth of the secondary flow velocities.

Similar characteristics are to be expected for an increase in the penetration angle while keeping the lobe height and wavelength constant. However, it should be noted that the effective size of the *AS* mixer is smaller compared to the *S* mixer, so that in a typical power plant installation, as, for example, in a turbofan engine exhaust, the contribution of the mixer to the overall weight of the engine would be less, but yet no compromise made on the mixing performance.

Acknowledgments

Financial support for this project from the Academic Research Fund and a Graduate Scholarship for T. H. Yip from the School of Mechanical and Production Engineering are gratefully acknowledged.

References

[1]Presz, W. M., Blinn, R. F., and Morin, B., "Short Efficient Ejector Systems," AIAA Paper 87-1837, Jan. 1987.

[2]Presz, W. M., Gousy, R., and Morin, B., "Forced Mixer Lobes in Ejector Design," *Journal of Propulsion and Power*, Vol. 4, No. 4, 1988, pp. 350–360.

[3]Presz, W. M., Reynolds, G., and McCormick, D., "Thrust Augmentation Using Mixer-Ejector-Diffuser Systems," AIAA Paper 94-0020, Jan. 1994.

[4]Paterson, R. W., "Turbofan Mixer Nozzle Flowfield—A Benchmark Experimental Study," *Journal of Engineering for Gas Turbines and Power*, Vol. 106, 1984, pp. 692–698.

[5]Barber, T., Paterson, R. W., and Skebe, S. A., "Experimental Investigation of Three-Dimensional Forced Mixer Lobe Flowfields," AIAA Paper 88-3785, Jan. 1988.

[6]Eckerle, W. A., Sheibani, H., and Awad, J., "Experimental Measurement of the Vortex Development Downstream of a Lobed Forced Mixer," *Journal of Engineering for Gas Turbines and Power*, Vol. 114, 1992, pp. 63–71.

[7]McCormick, D. C., and Bennett, J. C., Jr., "Vortical and Turbulent Structure of a Lobed Forced Mixer Free-Shear Layer," *AIAA Journal*, Vol. 32, No. 9, 1994, pp. 1852–1859.

[8]Yu, S. C. M., Yeo, J. H., and Teh, J. K. L., "Velocity Measurements Downstream of Lobed Forced Mixers with Different Convoluted Trailing Edge Configurations," *Journal of Propulsion and Power*, Vol. 13, No. 1, 1995, pp. 87–97.

[9]Weygandt, J. H., and Mehta, R. D., "Effects of Streamwise Vorticity Injection on a Plane Turbulent Wake," *AIAA Journal*, Vol. 33, No. 1, 1995, pp. 6–93.

[10]O'Sullivan, M. N., Waitz, I. A., Greitzer, E. M., Tan, C. S., and Dawes, W. N., "A Computational Study of Viscous Effects on Lobed Mixer Flow Features and Performance," *Journal of Propulsion and Power*, Vol. 12, No. 3, 1996, pp. 449–456.

[11]Manning, T. A., "Experimental Studies of Mixing Flows with Streamwise Vorticity," M.S. Thesis, Massachusetts Inst. of Technology, Cambridge, MA, Sept. 1991.

[12]Durst, F., Melling, A., and Whitelaw, J. H., *Principles and Practice of Laser Doppler Anemometry*, Academic, 1981.

[13]Maclaughlin, D. K., and Tiederman, W. G., "Biasing Correction for Individual Realization of the Laser Anemometry Measurements in Turbulent Flow," *Physics of Fluids*, Vol. 16, 1972, pp. 2082–2089.

[14]Yanta, W. J., and Smith, R. A., "Measurement of Turbulent Transport Properties with a Laser-Doppler Velocimeter," AIAA Paper 73-169, Jan. 1973.

[15]Yu, S. C. M., Xu, X. G., and Yip, T. H., "The Effects of Initial Boundary Layer Thicknesses to the Trailing Streamwise Vorticity in a Lobed Forced Mixer," *Journal of Propulsion and Power*, Vol. 14, No. 2, 1996, pp. 440–442.